Tellus
SERIES B
CHEMICAL
AND PHYSICAL
METEOROLOGY
PUBLISHED BY THE INTERNATIONAL METEOROLOGICAL INSTITUTE IN STOCKHOLM

Tellus (2010), 62B, 749–758

Side by side measurements of CO_2 by ground-based Fourier transform spectrometry (FTS)

By JANINA MESSERSCHMIDT[1]*, RONALD MACATANGAY[2], JUSTUS NOTHOLT[1], CHRISTOF PETRI[1], THORSTEN WARNEKE[1] and CHRISTINE WEINZIERL[1],
[1]*IUP, University of Bremen, Bremen, Germany;* [2]*University of Wollongong, Wollongong, Australia*

(Manuscript received 21 December 2009; in final form 28 June 2010)

ABSTRACT

High resolution solar absorption Fourier transform spectrometry (FTS) is the most precise ground-based remote sensing technique to measure the total column of atmospheric carbon dioxide. For carbon cycle studies as well as for the calibration and validation of spaceborne sensors the instrumental comparability of FTS systems is of critical importance. Retrievals from colocated measurements by two identically constructed FTS systems have been compared for the first time. Under clear sky conditions a precision for the retrieved xCO_2 better than ∼0.1% is demonstrated and the instruments agree within ∼0.07%. An important factor in achieving such good comparability of the xCO_2 is an accurate sampling of the internal reference laser. A periodic laser mis-sampling leads to ghosts (artificial spectral lines), which are mirrored images from original spectral lines. These ghosts can interfere with the spectral range of interest. The influence of the laser mis-sampling on the retrieved xCO_2 and xO_2 in the near-IR has been quantified. For a typical misalignment, the ratio of the ghost intensity compared to the intensity of the original spectral line is about 0.18% and in this case the retrieved xCO_2 is wrong by 0.26% (1 ppm) and the retrieved xO_2 is wrong by 0.2%.

1. Introduction

Carbon dioxide is the most important anthropogenic greenhouse gas. The spatial distribution and the temporal variation of the sources and sinks are insufficiently quantified. Information about sources and sinks of CO_2 are derived from atmospheric concentration measurements by inverse modelling. Up to now inverse modelling studies are mostly based on in situ boundary layer measurements. Recent studies (Stephens et al., 2007; Yang et al., 2007) showed that a large set of atmospheric inverse model results were inconsistent with total column measurements and vertical aircraft profiles as a result of incorrect vertical transport in the models. The column integral of CO_2 provides a largely independent piece of information to understand sources and sinks of CO_2. Source-sink estimates derived from these column measurements can be gravely distorted by small systematic biases in the measurements (Rayner and O'Brien, 2001). Therefore, a bias-free, spatially dense dataset must be established from satellite measurements, as well as a careful calibration and validation from the ground. For this reason the Total Carbon Column Observing Network (TCCON) has been established. It is a network of several sites around the globe, where the total column amount of carbon dioxide is measured by high resolution ground-based solar absorption Fourier transform spectrometry (FTS). With its current precision, FTS is the most suitable measurement technique for the calibration and validation of spaceborne column measurements of greenhouse gases. As a validation resource, the instrumental comparability of the FTS systems must be ensured. The comparability is of critical importance as an instrumental bias between different sites would cause a spurious spatial gradient, which would cause source/sink artefacts in inversion models. The FTS group at the University of Bremen is operating four measurement stations in Europe in the framework of the TCCON. The Bremen TCCON site had the unique situation to have for some time two FTS instruments: the permanent FTS instrument and a mobile FTS system, which was automated in Bremen. After construction, the mobile system was brought to Orléans, France in August 2009. In Bremen the instruments were operated in parallel and gave us the opportunity to study the influence of instrumental settings on the retrieved data and to compare measurements of nominally equivalent FTS instruments. A detailed description of the instrumental studies is given in Section 2. A laser mis-sampling in the commercially available FTS instruments was resolved in close cooperation with the manufacturer. In Sections 3 and 4 the influences of this technical problem on the retrieved data are

*Corresponding author.
Janina Messerschmidt, University of Bremen, Institute of Environmental Physics, Otto-Hahn-Allee 1, 28359 Bremen, Germany.
e-mail: messerschmidt@iup.physik.uni-bremen.de
DOI: 10.1111/j.1600-0889.2010.00491.x

discussed and summarized. After fixing this technical problem the results of the intercomparison of the two identical FTS instruments yield an excellent agreement and will be presented in Section 5. In Section 6, a summary and conclusion are given.

2. Instrumentation

2.1. Measurement Site: the FTS facility in Bremen, Germany

At Bremen (Germany, 53°N, 9°E) measurements have been started in 2000. Since 2004 the site is part of the networks NDACC and TCCON. While most European FTS observatories are located on high mountains, the FTS observations at Bremen are performed on flat terrain. The low altitude location is advantageous for studying tropospheric gases. In addition, the flat surroundings at the site in Bremen makes this site well suited for the validation of satellites.

2.2. Instrumental settings

Both instruments involved in the study are Bruker FTS 125HR spectrometers. A resolution of 0.014 cm^{-1} (defined as 0.9/*maximum optical path difference*), an aperture of 1 mm diameter and a scanner velocity of 10 kHz were used as standard parameters for the near infrared measurements. The electronic low pass filter is set to 10 kHz (≡15 798 cm^{-1}) and the high folding limit for the Fourier transformation to 15 798 cm^{-1}. An optical cut off filter at 15 800 cm^{-1} was additionally used to prevent aliasing. Optics User Software (OPUS) version 6.5, a program provided by Bruker, was utilized for the permanent TCCON instrument at the site in Bremen to record the spectra. In the mobile instrument, the raw data are obtained from the embedded web server (EWS) and the spectra are produced afterwards using SLICE-IPP, a software developed at Jet Propulsion Laboratory (JPL) in the United States. SLICE-IPP corrects the spectra for solar intensity variations, caused by passing clouds (Keppel-Aleks et al., 2007) as well. Both transformation approaches agree within the errors. GFIT (version 4.4.10), a non-linear least-square spectral fitting algorithm developed at JPL, was used for the retrieval of the trace gas column amounts from the measured spectra. A small difference of the instruments lies in the solar tracking system. The solar tracking system of the mobile FTS systems is fully automated. In the permanent instrument the solar tracking system is not automated and had to be manually realigned especially for high solar angles about every hour. Due to this monitoring both pointing errors lie within the acceptable range of 10% of the solar diameter.

2.3. Experimental setup

In the framework of two EU-projects, the *Global Earth Observation and Monitoring* (GEOmon) and the *Infrastructure for Measurements of the European Carbon Cycle* (IMECC), two fully automated FTS systems were built successively at the Institute of Environmental Physics (IUP) in Bremen, Germany. In the course of 2008 the first mobile FTS system for the site in Bialystok, Poland was automated. With this instrument, studies to estimate the influence of instrumental settings in 2008 were performed (Macatangay, 2008). In February 2009, this mobile FTS system was successfully installed in Bialystok, Poland. Afterwards, the mobile FTS system for the second site in Orléans, France was automated, referred to as F_FTS. Side by side measurements were performed with this mobile FTS system and the permanent FTS system (B_FTS) located in Bremen, Germany. This work will only focus on this comparability study.

2.4. Data analysis

The column-averaged dry-air mole fraction (DMF) of carbon dioxide, xCO_2, can be calculated from the retrieved column amount by

$$xCO_2(p) = \frac{column_{CO_2}}{[\frac{p_s}{m_{air}\,g} - column_{H_2O}]} \quad (1)$$

or by

$$xCO_2(O_2) = 0.2095 * \frac{column_{CO_2}}{column_{O_2}} \quad (2)$$

where p_s is the surface pressure, m_{air} is the mean molecular mass of air and g is the density-weighted gravitational acceleration.

The DMF xCO_2 is dimensionless and normally given in parts per million (ppm). The use of column concentrations of atmospheric molecular oxygen to determine the total dry column (eq. 2) minimizes systematic and correlated errors present in both the retrieved columns of CO_2 and O_2 (e.g. pressure errors, influence of the instrumental line shape (Washenfelder et al., 2006)).

A correction to the airmass dependence was applied. Data outside the ranges between 0.20 and 0.22 for CO_2 as well as outside 350 and 400 ppm for CO_2 were regarded as outliers. The CO_2 column is retrieved for two CO_2 bands centred at 6228 cm^{-1} and 6348 cm^{-1}. The average of the two calculated xCO_2 is presented here. Column xO_2 is retrieved from the electronic band centred at 7882 cm^{-1}.

The standard deviation of the $xCO_2(O_2)$ column measured during a 1-h clear sky period around local noon is used as a measure of precision. The criterion for comparability is when the $xCO_2(O_2)$ abundance retrieved from one FTS instrument falls within the range of precision of the other instrument.

3. Initial intercomparison of two FTS instruments

Figure 1 illustrates systematic differences between the instruments, which are greater than the precision for all retrieved

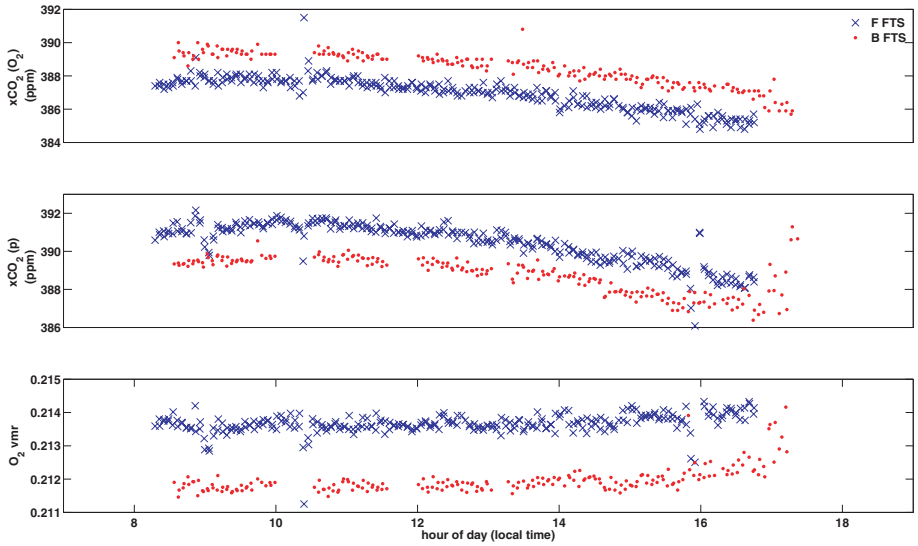

Fig. 1. Initial comparison of two nominally equivalent FTS systems with a systematic error. Due to an internal laser mis-sampling, phase ghosts are aliased in the spectral regions of interest. The xO_2 retrieval is more affected by the systematic mis-sampling than the CO_2 retrieval and so the effect does not cancel in the $xCO_2(O_2)$ ratio. The measurements of the permanent instrument B_FTS are shown as dots. The data of the mobile instrument F_FTS are indicated with crosses.

gases. Good agreement between the instruments could only be achieved after correcting a systematic laser mis-sampling. Without correction of this fault, systematic differences between the data of the nominally equivalent instruments were observed and the comparability could not be ensured.

As exemplified in Fig. 1 all retrieved data showed a nearly constant offset despite cloud free weather conditions, well aligned and identical FTS systems. The mean differences and precisions are outlined in Table 1. The precision is similar described by Washenfelder et al. (2006). As the difference of the two instruments is much higher than the precision, it can be concluded that the data are not comparable. Similar results are also found for all other days. It was likely that these offsets are systematic and not caused by a anomalous event on a single day.

Possible causes like misalignment of the laser or the optics would be seen in the instrumental line function, errors in the tracker pointing would be seen in the data as a function of the solar zenith angle, interference of other gases would be seen in the residuals. As the instrument were well aligned, the offsets were not a function of time and the residuals looked inconspicuous, these explanations could not be the reason for the offsets.

Table 1. Precision of the FTS instruments during a 1-h period of cloud free weather conditions are given. The differences between the FTS systems with and without an adjusted laser mis-sampling are shown as well. As it can be seen the comparability of the $xCO_2(O_2)$ improves significantly for the adjusted laser mis-sampling. The unaltered differences for the $xCO_2(p)$ and the xO_2 can be explained by a pointing problem in the mobile FTS system F_FTS. The pointing error affects both gases the same way and cancels out in the $xCO_2(O_2)$.

	$xCO_2(O_2)$	$xCO_2(p)$	xO_2
precision	0.1%	0.09%	0.1%
without ghosts			
Δ FTS	0.07%	0.72%	0.89%
	0.27 ppm	2.77 ppm	0.0019
with ghosts			
Δ FTS	0.44%	0.41%	0.85%
	1.70 ppm	1.60 ppm	0.0018

4. Influence of Phase Ghosts on FTS measurements

The difference could be understood and corrected after finding spectral lines from the near infrared aliased into the visible range shown in Fig. 2. Aliasing means that due to the measurement process spectral features are mirrored into other spectral regions. Figure 2 shows a solar absorption measurement recorded with the TCCON standard settings but with an high folding limit (HFL) of 31 596 cm^{-1}. This HFL is not used for TCCON purpose, but the figure is shown here because the real signal at ∼23 600 cm^{-1} is negligible compared with an artificial signal in this range, allowing the latter to be seen directly. This signal looks exactly like the spectral lines in the near infrared range and are called ghosts. These ghosts are difficult to see in spectra taken with TCCON settings (i.e. broad bandpass, HFL = 15 798 cm^{-1}) as they are superimposed onto the original spectrum. Only in special situations when the spectrum contains wide

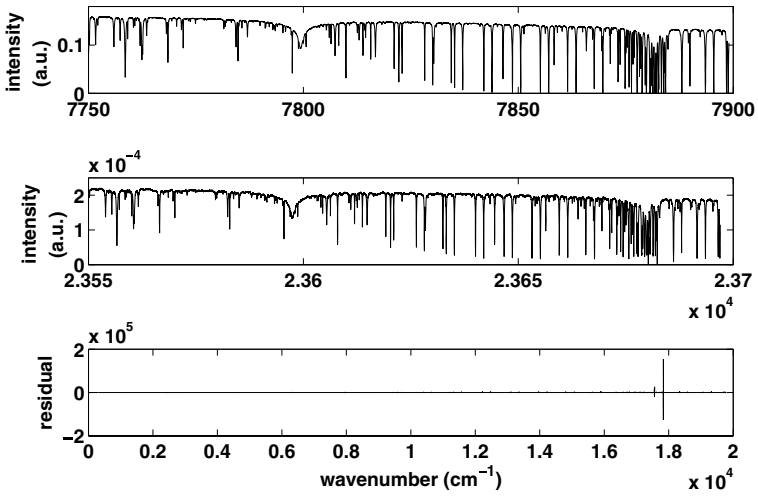

Fig. 2. The figure shows ranges of a solar spectrum taken with TCCON standards, but an HFL of 31 596 cm^{-1}. The measurement is shown because ghosts can be seen with the higher HFL. As the real signal at $\sim$23 600 cm^{-1} is negligible compared with the ghosts, latter can be seen directly. They are exactly the same like the original lines around 7885 cm^{-1}, only reduced in intensity ($\sim$0.13%). The back folding into the spectral ranges of interest sensitively changes the retrieval of xCO_2 and xO_2.

regions with no true signal can the ghosts be directly observed. There are two ways of achieving this: use of a narrow bandpass filter or increasing the HFL to 31 596 cm^{-1}. In the Appendix A1 an experimental setup is described to test for ghosts in an FTS instrument. In the following section ghosts are introduced and the influence on the retrieved gases will be discussed.

4.1. Theory of phase ghosts

According to Guelachvili (1981) systematic errors in FTS can be classified in three different specific groups. The first encompasses errors which are caused by the addition of a systematic signal during the recording of the interferogram. The second refers to interferogram phase distortions and the third to errors where the intensity of the interferogram is perturbed. The first is an Additive Error and the two latter are referred to as Multiplicative Errors. The ghosts seen in the shown measurements (Fig. 1) can be attributed to the second case and will be discussed more closely in this work.

In FTS the interferogram needs to be sampled equally in optical path difference (OPD). An internal HeNe-laser is used to define the sampling points: the zero crossings of the laser interferogram determine the sampling points. If the zero crossings are not defined correctly (e.g. due to a time delay problem in the electronic signal processing or an constant offset in the amplifier chain), the sampling points are not equidistant in OPD. This causes a periodic error in the sampling intervals (Fig. 3). The Fourier transformation of an asymmetric sampled interferogram has ghosts, antisymmetric spectral signals on each site of every spectral line shifted by the period of the sampling error. In our case the period of the sampling error is identical to the laser frequency and therefore the ghosts appear 15 798.022 cm^{-1} above and below the parent lines in the spectra. The intensity of the ghosts is proportional to the sampling error and the parent line. These ghosts can be aliased into a spectral region being used for analysis of gases, causing a systematic error in the retrieved columns.

Guy Guelachvili formulate this relationship as follows: A periodic error in the path difference is described as

$$\epsilon = \epsilon_0 \sin(2\pi\beta\Delta + \Phi_o) \tag{3}$$

(Guelachvili, 1981), page 25

with β: period of error, Δ: sampling step and Φ_o: an additive factor. If $\Phi_0 = 0$ is assumed and ϵ_o is small, the Fourier Transformation of such a disturbed interferogram leads to a spectrum, in which the parent spectral line plus a response multiplied by a factor $\pm\pi\sigma_0\epsilon_0$ and located at $\sigma_0 \pm \beta$ is obtained (with: σ_0 wavenumber of parent line):

$$\begin{aligned} B'(\sigma) = {} & J_0(2\pi\sigma_0\epsilon_0)\int_0^{\Delta_M} \sin 2\pi\sigma_0\Delta \sin 2\pi\sigma\Delta d\Delta \\ & + \sum_{k=1}^{\infty} J_k(2\pi\sigma_0\epsilon_0)\int_0^{\Delta_M} [\sin 2\pi(\sigma_0 + k\beta)\Delta \\ & + (-1)^k \sin 2\pi(\sigma_0 - k\beta)\Delta] \sin 2\pi\sigma\Delta d\Delta \end{aligned} \tag{4}$$

(Guelachvili, 1981), page 25

with J_k: Bessel's function and k: 1, 2, ... n.

The eq. (4) shows that the parent line is multiplied by a numerical factor smaller than one and that therefore the intensity of the parent line decreases in the presence of ghosts. This means that the laser mis-sampling has two effects on the spectral lines: Not only can ghosts be folded back from aliased regions into the region of interest, but the intensity of the original lines decreases as well.

Additionally to the first order of ghosts, higher order of ghosts appear at $\pm 2\beta$, $\pm 3\beta$, ..., $\pm n\beta$, with smaller intensities. Depending on the parity of n these features have antisymmetric (n odd) or symmetric (n even) shapes centred on the parent line.

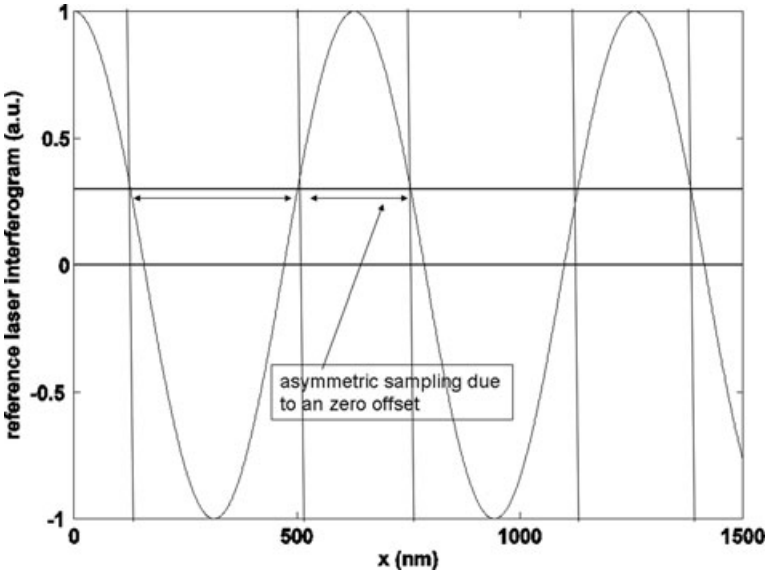

Fig. 3. A reference laser interferogram is shown with and without a mis-sampling. The zero points of the laser signal are taken as reference for the sampling of the measurements. Due to the zero offset an asymmetric sampling is caused, which leads to phase ghosts. These ghosts are aliased into the spectral regions of interest and affect the gas retrieval.

Guelachvili (1981) as well as Learner et al. (1996) point out that the position of the ghosts depend on the period of the error β, which depends on the sampling rate per laser wavelength. The setting of the high folding limit (HFL) determines the sampling rate per wavelength, and therefore the period of the error β. For example, if the HFL is set to 15 798 cm^{-1}, the interferograms are sampled twice per laser wavelength (as illustrated in Fig. 3) and the ghosts occur at $\sigma_0 + \beta$ and $\sigma_0 - \beta$ and are both aliased to the same frequency: $\beta - \sigma_0$. If the HFL is set to 31 596 cm^{-1}, the interferograms are sampled four times per laser wavelength and the negative ghost is aliased to $\beta - \sigma_0$, but the positive ghost is found (unaliased) at $\beta + \sigma_0$. If the HFL is set to 7899 cm^{-1}, the interferograms would be sampled only once per laser wavelength and the sampling would always be uniform (no ghosts). But an HFL of 7899 cm^{-1} would not allow measurements of the O_2 band.

It is to point out that even if an antialiasing filter is used the phase ghosts at negative frequencies can be aliased in the spectral region of interest. It is therefore important to adjust laser mis-sampling in the instrument. In Section A1 an experimental setup is shown to adjust the laser mis-sampling.

In Section A2 an experiment is described, with which the influence of the ghosts on the retrieved gases was quantified. A linear fit (Fig. 4) to the data shows that a ratio of a ghost to its parent line of 0.18% leads to an over- or underestimation of 1 ppm in the xCO_2. With the test setting from section A1 the ratios for both instruments were estimated. Applying the relationship of the linear fit gives the influence of the ghosts for the specific instruments (Table 2). With this estimation the measured difference of 1.7 ppm in the $xCO_2(O_2)$ can mostly (1.12 ppm $\equiv \sim$66%) be explained with the laser mis-sampling. The corresponding values for the $xCO_2(p)$ values and the O_2 values can be found in Table 2. In summary, the laser mis-sampling can explain a high fraction of the offset in the $xCO_2(O_2)$ data and partly the $xCO_2(p)$ and xO_2 differences. The rest is likely to be due to instrumental errors (e.g. solar tracking errors, instrumental line shape errors). Further discussion are made in section 5. Variations of the difference between different days can be explained by varying conditions for example in interfering H_2O lines.

4.2. *The varying influence of the ghosts on the retrieved gases*

A short calculation can show that the xO_2 retrieval will be more affected than the xCO_2 retrieval: With the used settings and a laser mis-sampling, phase ghosts of lines around 7885 cm^{-1} can be found at 23 683 cm^{-1} and at -7913 cm^{-1}. These ghosts are folded back in the range of $+7913$ cm^{-1}, which lies in the range for the O_2 retrieval. As mentioned, Fig. 2 shows a spectrum recorded with the B_FTS instrument and an HFL of 31 596 cm^{-1}. It can be derived from this figure that for the B_FTS instrument the intensity of the ghosts, which will be aliased in the retrieval ranges are around 0.13% of the original spectrum. As the lines around 7913 cm^{-1} and the lines in the range of 7885 cm^{-1} have an intensity level of 0.15, the intensity of the aliased ghosts lies around 0.13% of the atmospheric lines and will have a significant influence on the O_2 retrieval (Fig. 5).

The influence on the retrieved $xCO_2(p)$ is much smaller due to the ratio of the intensity of the ghosts and the relevant atmospheric range. For the retrieved $xCO_2(p)$ in the 6220 cm^{-1} band the ghosts are aliased from the spectral range around 9578 cm^{-1}. In this range the intensity of the atmospheric signal lies around 0.06. The intensity in the 6220 cm^{-1} is around 0.35 (Fig. 6). Therefore the intensity of the ghosts in the 6220 cm^{-1} band lies only around 0.02% of the atmospheric lines in this range. These

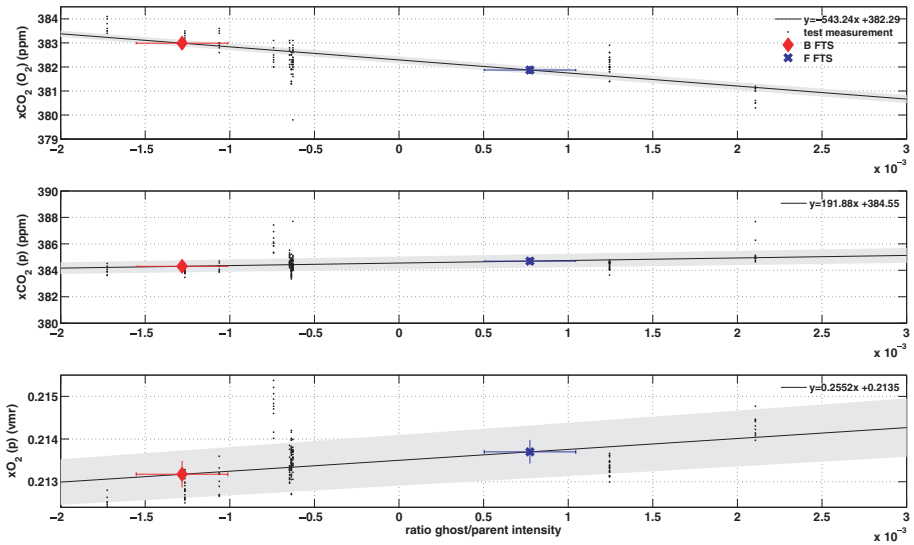

Fig. 4. The retrieved $xCO_2(O_2)$, $xCO_2(p)$, xO_2 DMF are shown as a function of the ratio of the amplitudes of the ghosts and the parent lines. The dependence of the retrieved gases leads to over- or underestimating of the gases in the retrieval. With these linear, empirical relationships and the knowledge of the amplitude of potential ghosts, existing xCO_2 measurements can be corrected for the presence of ghosts.

Table 2. The table shows the slopes and intercepts of the linear relationships between the retrieved gases and the ratio of the ghosts to the parent line. They were derived from the measurements presented in Fig. 4 and explained in Section A2. The influence of the ghosts for both instruments and the resulting differences in the comparison study are shown as well.

	$xCO_2(O_2)$	$xCO_2(p)$	xO_2
m	−543.24	191.88	0.2552
b	382.29	384.55	0.2135
$\frac{m}{b}$	1.42	0.50	1.20
influence of ghosts:			
on B_FTS	−0.70 ppm	−0.25 ppm	−0.0003
on F_FTS	0.42 ppm	0.15 ppm	0.0002
on ΔFTS	1.12 ppm	0.4 ppm	0.0005
(see Table 1)	66% ΔFTS	25% ΔFTS	28% ΔFTS

effects can clearly be seen in the data. The difference between the xO_2 values is more significant than of the $xCO_2(p)$ values.

5. Intercomparison of two identical FTS instruments

The intercomparison of two identical FTS instruments, which are corrected for laser mis-sampling, will be discussed using the measurements on 27 July 2009. The instruments were well aligned, the laser mis-sampling were adjusted and they were measuring with the same parameters as described in section 2. All measurements show differences in the $xCO_2(p)$ and xO_2 values, but a very good agreement in the $xCO_2(O_2)$ values (Table 1, Fig. 7). The difference between the $xCO_2(O_2)$ of the two instruments is around 0.07% and better than the precision of 0.1% (Table 1). The agreement of the $xCO_2(O_2)$ is typical for all other cloud free days. Therefore, it can be concluded that the comparability between the instruments meets the requirements. Investigating the xO_2 and $xCO_2(p)$ individually, Table 1 shows that the difference is much higher than the precision. Therefore these results are not comparable. The differences are basically due to an error in the solar tracking system of the F_FTS. Concerning the quality of the solar tracking a suitable indicator is the pointing error, which is the deviation from pointing at the middle of the sun and can be estimated by the Doppler Shift. Figure 8 shows an anomalous high pointing error up to 0.1° for this day. This pointing error will lead for an airmass of 1.5 to an error in the retrieval of about 0.26% ($\frac{=1.5\times0.1\,\pi}{180)}$). This estimation will only show deviations from the axis of rotation and the pointing error can even be higher. Therefore at least 36% of the difference in the $xCO_2(p)$ and 30% of the differences in the xO_2 can be explained by the pointing error. Additionally other errors, like misalignment of the instrument, errors in the linelists will sum up. The important point is that these errors, which affect the O_2 and the CO_2 in the same way (e.g. pointing error or individual instrumental line shape) cancel out in the $xCO_2(O_2)$. In the case of ghosts the influence on the gas retrieval does not cancel out and still affects the $xCO_2(O_2)$ retrieval. Therefore it is important to adjust FTS instruments for potential ghosts.

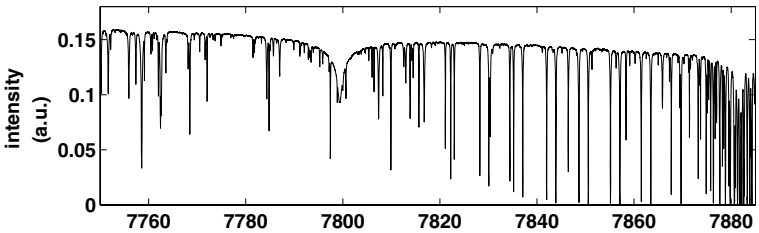

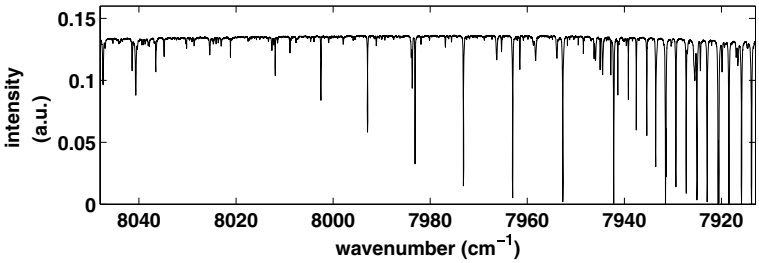

Fig. 5. The spectral range of the xO_2 retrieval (7885 cm^{-1} band) and the region where the interfering ghosts arises from (7913 cm^{-1}) are shown. It can be seen that the intensity level of the lines in both regions are similar. As the ghosts have an intensity of 0.13% of the original spectrum (Figure 2), they will influence the xO_2 retrieval with an intensity of 0.13% compared to the original lines.

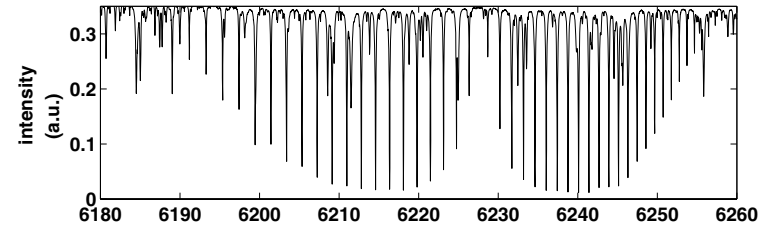

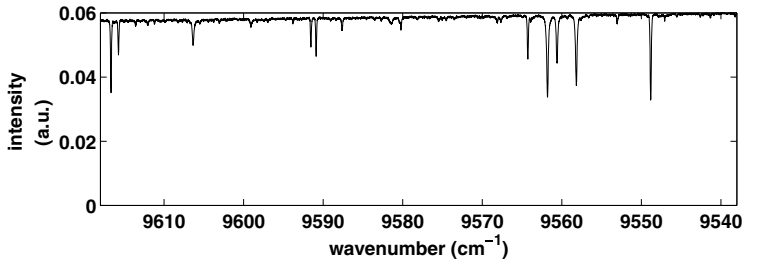

Fig. 6. Like in Fig. 5 the CO_2 lines in the 6220 cm^{-1} retrieval band and the region where the interfering ghosts arises from (9578 cm^{-1}) are shown. It can be seen that unlike for the xO_2 the intensity level in the region of 9578 cm^{-1} is much smaller than the intensity level of the retrieval region. Therefore the CO_2 retrieval will be much less affected from the aliased ghosts.

6. Conclusion

A precision about ∼0.1% was demonstrated and the comparability of FTS instruments for $xCO_2(O_2)$ could be estimated about ∼0.07%. These values confirm the suitability of the TCCON as a validation resource for satellite measurements. The demonstrated comparability reduces a potential risk of systematic bias between different sites, which would cause spurious spatial gradients and therefore source/sink artefacts in inversions. Well aligned and adjusted FTS systems are suitable for satellite and model comparison, in which they give an independent piece of information on carbon cycle processes.

The comparability could only be ensured by aligning a systematic laser mis-sampling. This means that the elimination of the laser mis-sampling is crucial for the high quality of FTS measurements. As the influence of the ghosts does not cancel out in the data product $xCO_2(O_2)$, like in the case of instrumental errors, it is important to eliminate the source of ghosts. As the influence of ghosts was estimated in the range of ppm, the authors suggest a ghost correction step in the retrieval software for past measurements.

7. Acknowledgments

We acknowledge the support of the European Commission within the 6th Framework Program through the Integrated Infrastructure Initiative IMECC (Infrastructure for Measurement of the European Carbon Cycle) and the Integrated Project GEOmon (Global Earth Observation and Monitoring). We thank Frank Hase (Forschungszentrum Karlsruhe, Germany), David Griffith (University of Wollongong, Australia), Geoffrey C. Toon (Jet Propulsion Laboratory, U.S.), Debra Wunch (California Institute of Technology, U.S.) and Nina Rauhut (Institute of

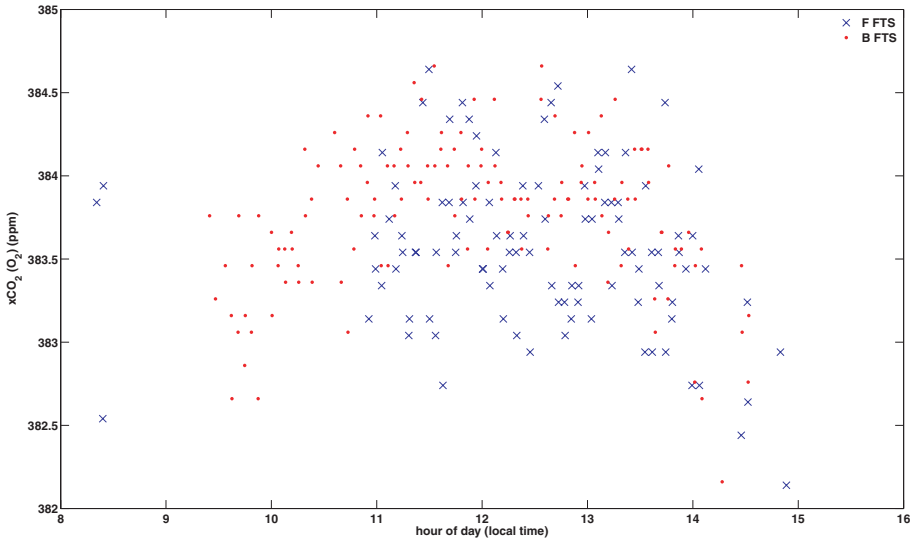

Fig. 7. Comparison of two nominally equivalent FTS instruments with an adjusted laser sampling. The $xCO_2(O_2)$ agrees very well ($\sim 0.07\%$ difference). The differences in the $xCO_2(p)$ and xO_2 retrieval are likely to be due to a solar tracking problem of the mobile instrument. The data of the permanent FTS system (B_FTS) are shown as dots. The data of the mobile instrument (F_FTS) are indicated by crosses.

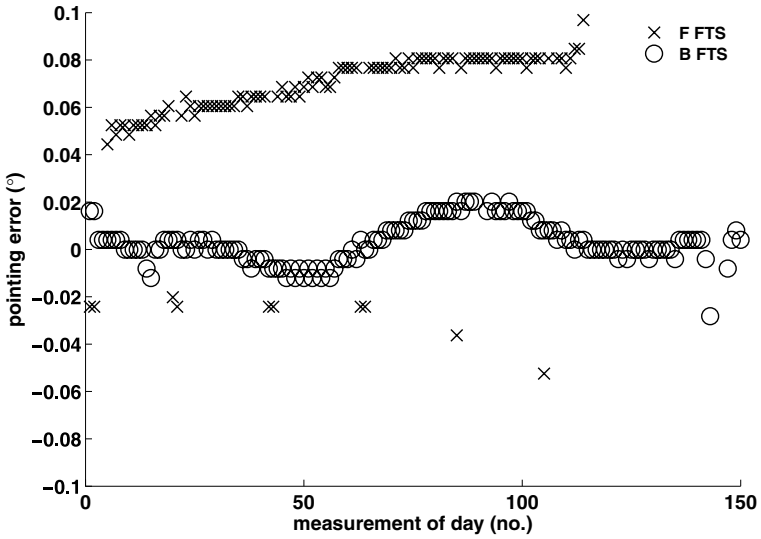

Fig. 8. The pointing error for the permanent instrument B_FTS and the mobile instrument F_FTS are shown for the 27 July 2009. The pointing error for the mobile systems lies within $-0.06°$–$0.06°$ [$\sim$1.05 mrad] and the pointing error for the permanent systems lies around $-0.04°$–$0.04°$ [$\sim$0.70 mrad]. The pointing error of the mobile system is likely to cause the differences in the retrieval. For comparison, the solar disc has a diameter of $0.533°$ [$\sim$9.3 mrad].

Environmental Physics, Germany) for helpful discussions and suggestions for improvement.

8. Appendix: Experimental setups to estimate the influence of the ghosts

A.1. A test setup for adjusting the laser mis-sampling

As pointed out in Section 3 ghosts are difficult to see in the standard experimental setup of TCCON. Therefore a method to estimate potential ghosts in the FTS is introduced. By recording spectra of an internal lamp using a narrow-band filter around 4140 cm^{-1}, with an internal HeNe-Laser (632.8 nm) and sampling at every zero crossing (HFL = 15 798 cm^{-1}) a laser mis-alignment can be shown and quantified. According to eq. (3), a ghost should be seen at 11 658 cm^{-1} (= |4140 cm^{-1} 15 798 cm^{-1}|) in case of a laser mis-alignment ($\sigma_o = 4140\,cm^{-1}$ and $\Delta = 316.4$ nm) (Fig. 9).

A secondary peak at 8300 cm^{-1} can be seen in Fig. 9 as well. This second peak is due to detection non-linearity. This feature would lead to a zero level offset in a broadband solar spectrum, but won't affect the xCO_2 in the way the comparatively tiny ghost peak at 11 658 cm^{-1} will. The difference between the detection non-linearity and the laser mis-sampling is that the latter carries

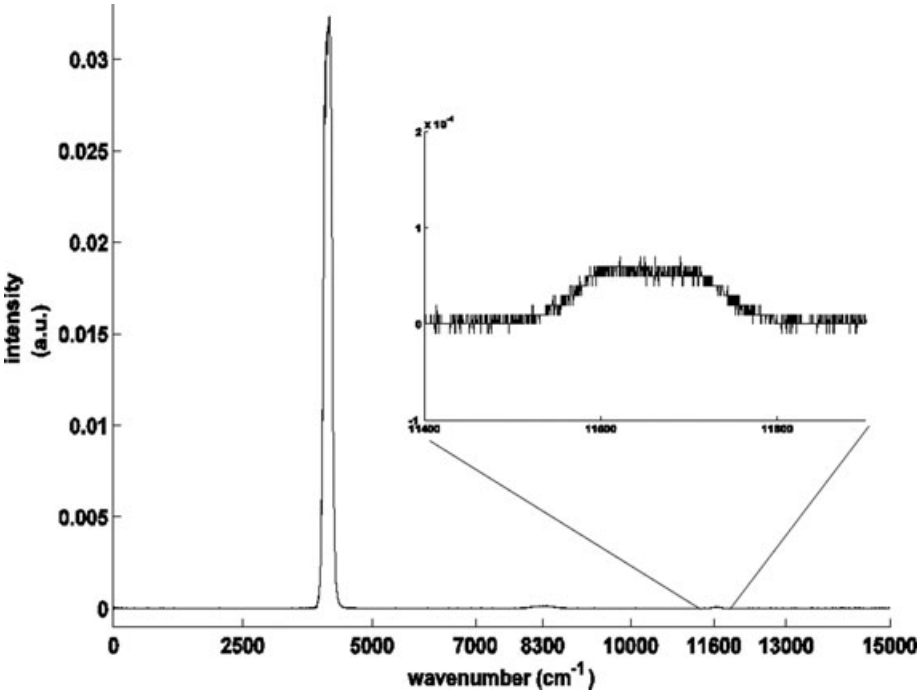

Fig. 9. A spectrum taken with an internal lamp and a narrowband filter around 4140 cm^{-1} is shown. In the spectrum, an artifical signal is found at 11 658 cm^{-1}, which appears due to a laser mis-sampling of the internal reference laser. The second peak at 8300 cm^{-1} is likely to be due to an detector nonlinearity and won't affect the retrieval as much as the comparatively smaller ghosts, but will lead to an zero offset in the spectra.

high-resolution spectral information whereas the detection nonlinearity causes only an intensity offset. The following example explains the influence of the ghosts:

Ghosts transfer spectral energy for example from 4140 cm^{-1} to 11 658 cm^{-1}, as illustrated in Fig. 9, but they will transfer energy in the reverse direction as well. In the case of Fig. 9, there is no real signal at 11 658 cm^{-1} due to the narrow bandpass filter, so there is no corruption of the spectrum at 4140 cm^{-1}. But in the case of a broad bandpass solar spectrum, there will be real signal at 11 658 cm^{-1}, a fraction of which will be aliased into the 4140 cm^{-1} region. Similarly, a fraction of the real spectral signal at 9598 cm^{-1} will be aliased to 6200 cm^{-1} and interfere the CO_2 retrieval.

The potential ghost visualized in the test setup can be eliminated with an alignment board provided by Bruker. On the alignment board is a potentiometer, with which the ghosts can be adjusted. It is important to use hereby the scanner velocity normally used in the measurements, because the scanner velocity has an influence on the intensity of the ghosts as well (Fig. 10).

A.2. Dependency of the ghosts on the laser mis-sampling and on the scanner velocity

Ghosts are dependent on the scanner velocity and the beamsplitter, because the amplitude of the laser interferogram changes with their selection. The higher the scanner velocity, the smaller the amplitude of the laser interferogram and the larger the ratio of the mis-sampling to the sampling step (eq. 3). Following two experimental setups analyze the dependency of the ghosts on the quantity of the mis-sampling and on the scanner velocity.

At first solar absorption measurements were performed with different settings of the potentiometer on the alignment board at clear days (14 and 15 October 2009) with the B_FTS instrument at the Bremen site, Germany. In Fig. 4 the retrieved $xCO_2(O_2)$, $xCO_2(p)$ and xO_2 are plotted against the ratio of the ghost to the parent line. A linear fit, $m \times x + b$, was applied to the data and the values for m and b are shown in Table 2. Fig. 4 shows that the $xCO_2(O_2)$ changes about 1 ppm for a ratio of 0.18%. The $xCO_2(p)$ changes about 1 ppm for a ratio of 0.52% and the xO_2 values changes about 1% for a ratio of 0.82%. With these relationships existing solar absorption measurements can be corrected, if the ratio of the ghosts to the parent lines is known for the instruments. With the test measurement described in section A1 the ratios were calculated for both instruments. The laser mis-sampling of the permanent Bremen instrument corresponds to a ratio of 0.13% and for the F_FTS instrument to a ratio of 0.08%. For the B_FTS instrument an offset of 0.7 ppm $\pm$ 0.13 $xCO_2(O_2)$ and for the F_FTS an offset of minus 0.42 ppm $\pm$ 0.15 due to the laser mis-sampling was found. The corresponding values for the $xCO_2(p)$ and xO_2 are written in Table 2.

To study the influence of the scanner velocity on the ghosts several tests were performed: Potential ghosts were adjusted

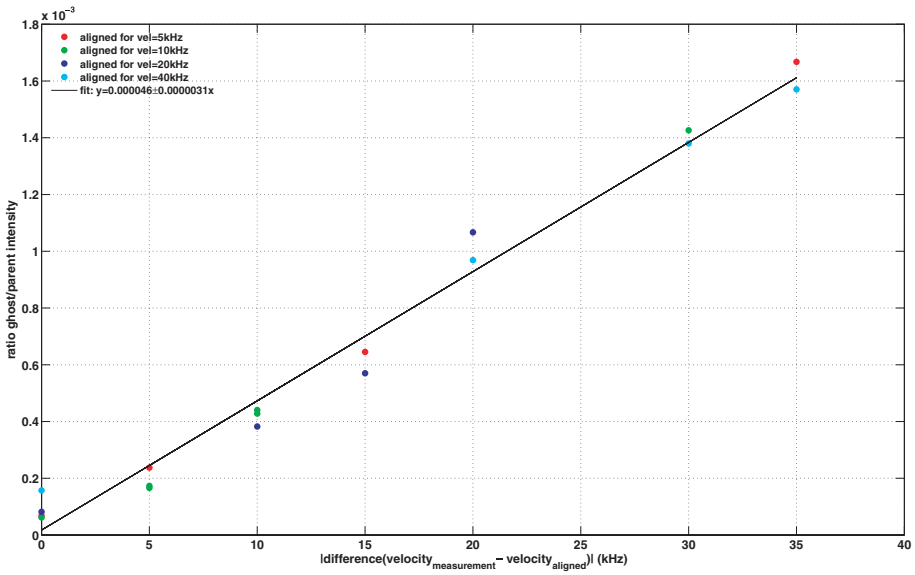

Fig. 10. Ghost amplitudes are shown as a function of the difference between the scanner velocity at which a measurement was done and the velocity at which the ghosts were minimized by adjusting the laser potentiometer. For example, potential ghosts were minimized during measurements, introduced in section A1, with a scanner velocity of 10 kHz. Then test measurements were taken with 5, 20 and 40 kHz and the ratios of resulting ghosts to their parents were recorded. The figure shows that the ratio is only dependent on the difference of the velocities and not on the absolute value.

at a specific scanner velocity (e.g. 10 kHz) with the test measurements described in Section A1. Then test measurements were taken successively with scanner velocities of 5, 10, 20 and 40 kHz and the ratio of potential ghosts and their parents were recorded. These measurements were repeated for adjusted ghost for each velocity. The results are shown in Fig. 10. The figure shows that the ratio is only dependent on the difference of the scanner velocity of the measurement and the velocity at which the ghosts were adjusted and not on the absolute value of the velocity.

References

Guelachvili, G. 1981. Distortions in Fourier spectra and diagnosis. In: *Spectrometric Techniques*, Volume 2, Academic Press, New York, 1–61. ISBN 9780127104027.

Keppel-Aleks, G., Toon, G. C., Wennberg, P. O. and Deutscher, N. M. 2007. Reducing the impact of source brightness fluctuations on spectra obtained by fourier-transform spectrometry. *Appl. Opt.* **46**(21), 4774–4779.

Learner, R. C. M., Thorne, A. P. and Brault, J. W. 1996. Ghosts and artifacts in fourier-transform spectrometry. *Appl. Opt.* **35**(16), 2947–2954.

Macatangay, R. 2008. *Atmospheric Carbon Dioxide: Retrieval from ground-based Fourier transform infrared solar absorption measurements and modelling using a coupled global-regional scale approach*. PhD thesis, University of Bremen, Germany.

Rayner, P. J. and O'Brien, D. M. 2001. The utility of remotely sensed CO_2 concentration data in surface source inversions. *Geophys. Res. Lett.* **28**(1), 175–178. doi:10.1029/2000GL011912.

Stephens, B. B., Gurney, K. R., Tans, P. P., Sweeney, C., Peters, W. and co-authors. 2007. Weak northern and strong tropical land carbon uptake from vertical profiles of atmospheric CO_2. *Science* **316**(5832), 1732–1735. doi:10.1126/science.1137004.

Washenfelder, R. A., Toon, G. C., Blavier, J.-F., Yang, Z., Allen, N. T. and co-authors. 2006. Carbon dioxide column abundances at the Wisconsin tall tower site. *J. Geophys. Res.* **111**, 1–11. doi:10.1029/2006JD007154.

Yang, Z., Washenfelder, R. A., Keppel-Aleks, G., Krakauer, N. Y., Randerson, J. T. and co-authors. 2007. New constraints on northern hemisphere growing season net flux. *Geophys. Res. Lett.* **34**. doi:10.1029/2007GL029742.